ELSEVIER

International Journal of Heat and Fluid Flow 20 (1999) 368–373

International Journal of HEAT AND FLUID FLOW

www.elsevier.com/locate/ijhff

Simulation and Reynolds stress modeling of particle-laden turbulent shear flows

D.B. Taulbee [a,*], F. Mashayek [b], C. Barré [a]

[a] Department of Mechanical and Aerospace Engineering State, University of New York at Buffalo, Buffalo, NY 14260-4400, USA
[b] Department of Mechanical Engineering, University of Hawaii at Manoa, 2540 Dole Street, Honolulu, HI 96822, USA

Received 5 February 1998; accepted 1 March 1999

Abstract

Direct numerical simulation (DNS) is conducted of a homogeneous turbulent shear flow laden with mono-size particles. The dispersed phase is simulated in the Lagrangian frame and the carrier phase is considered in the Eulerian manner. The coupling between the two phases is 'two-way' which allows investigation of the effects of the mass loading ratio and the particle time constant on both phases. A new Reynolds stress model (RSM) is developed based on a 'two-fluid' methodology in which both the carrier phase and the dispersed phase are considered in the Eulerian frame. Closures are suggested for the unclosed terms (including the pressure–velocity gradient) which manifest the effects of two-way coupling. The results generated by DNS are used to determine the magnitudes of some of the empirical constants appearing in RSM. The final model predictions for all the components of the fluid, the particle, and fluid-particle Reynolds stresses are assessed via detailed comparisons against DNS data.

1. Introduction

A variety of statistical models are available for predictions of multiphase flows (Crowe et al., 1996). A large number of investigations are based on the Eulerian description utilizing turbulence closures for both the dispersed and the carrier phases. The closure schemes for the carrier phase are mostly limited to 'Boussinesq' type approximations in conjunction with modified forms of the conventional k–ϵ (e.g. Elghobashi and Abou-Arab (1983)). The models for the dispersed phase are typically via the 'Hinze–Tchen' algebraic relation (Chen and Wood, 1986) which relates the eddy viscosity of the dispersed phase to that of the carrier phase. While the simplicity of this model has promoted its use, its universality has not been recognized. Hence, there is a need to develop more general closure models for two-phase flows.

The objective of this work is twofold: (1) conduct DNS of particle-laden turbulent shear flows and (2) provide a new second-order Reynolds stress model for statistical predictions of two-phase flows. While the DNS results are used to investigate some physical issues pertaining to the structure of such flows, their primary use is to aid the development of RSM. The model is associated with the Reynolds stresses in both phases and the cross-correlation between the velocities of the two phases. Some of the previous contributions in such modeling are due to Shih and Lumley (1986) who present a second order theory for particle dispersion with small-inertia particles and Simonin et al. (1995) who develop a second moment model theory with one-way coupling. Zhou et al. (1994) also consider a second order theory but do not present a closed set of transport equations for the second moments. Here, DNS data are used rather extensively for both model parameterization (determination of some of the empirical constants appearing in the model), and model assessments. The RSM as proposed here is in the form of full second order transport equations.

One of the first implementations of DNS in two-phase flows is due to Riley and Patterson (1974) who investigate particle dispersion in isotropic turbulence. McLaughlin (1989) simulates particle deposition in a channel, and Squires and Eaton (1991a, b) have conducted extensive DNS of stationary and decaying turbulence fields with one- and two-way coupling. Elghobashi and Truesdell (1992, 1993) report the results of similar studies. While there are no reported DNS results on particle-laden homogeneous turbulent shear flows, several large eddy simulation (LES) results of such flows are available (Yeh and Lei, 1991; Simonin et al., 1995). These studies have been very useful for understanding the physics of particle-laden shear flows and for assessment of some of the recent theories pertaining to such flows (Reeks, 1993; Liljegren, 1993). However, the uncertainties associated with the subgrid scale closures as used in LES, does not allow for a through assessment of turbulence closures. This assessment is better furnished via DNS.

2. Direct numerical simulation

The governing equations considered here are the continuity and Navier–Stokes equations for the continuous fluid phase,

* Corresponding author.

0142-727X/99/$ – see front matter
PII: S0142-727X(99)00028-4

coupled with the Lagrangian equations for discrete particles. The particles are assumed to be spherical with diameter smaller than the smallest length scale of the turbulence and to obey an empirically corrected Stokesian drag relation. The particle density is much larger than the fluid density such that only the drag force is significant to the particle dynamics. In addition, the particle volume fraction is assumed to be relatively small and particle–particle interactions are neglected. The fluid velocity and pressure are denoted by $\hat{U}_i$ and $\hat{P}$, and the particle position and velocity are denoted as X_i and $\hat{V}_i$, respectively, where the hat $\hat{}$ indicates the instantaneous quantity. With this nomenclature, the continuity and momentum equations for the fluid, and the Lagrangian equations of motion for a single particle are given by:

$$\frac{\partial \hat{U}_j}{\partial x_j} = 0, \tag{1}$$

$$\frac{\partial \hat{U}_i}{\partial t} + \frac{\partial}{\partial x_j}(\hat{U}_i \hat{U}_j) = -\frac{1}{\rho_f}\frac{\partial \hat{P}}{\partial x_i} + \frac{1}{\nu}\frac{\partial^2 \hat{U}_i}{\partial x_j \partial x_j} - \frac{1}{\rho_f \Delta V}\sum^{n_p}\left\{\frac{f m_p}{\tau_p}(\hat{U}_i^* - \hat{V}_i)\right\}, \tag{2}$$

$$\frac{dX_i}{dt} = \hat{V}_i, \quad \frac{d\hat{V}_i}{dt} = \frac{f}{\tau_p}(\hat{U}_i^* - \hat{V}_i), \tag{3}$$

where x_i and t are the spatial and temporal coordinates, respectively, and ρ_f and ν are the fluid density and kinematic viscosity, respectively. The particle time constant for Stokesian drag of a spherical particle is $\tau_p = \rho_p d_p^2/18\mu$, where ρ_p and d_p are the particle density and diameter, respectively, and μ is the fluid viscosity. The function $f = 1 + 0.15\ \mathrm{Re}_p^{0.687}$ in Eqs. (2) and (3) represents an empirical correction to Stokesian drag for large particle Reynolds numbers ($\mathrm{Re}_p = \rho_f^* d_p |\hat{U}_i^* - \hat{V}_i|/\mu$) and is valid for $\mathrm{Re}_p \leqslant 1000$. The superscript $(*)$ indicates the values of the fluid variables at the particle location. The last term in Eq. (2) represents the effects of the particle drag which is calculated by volume averaging the contributions from all of the individual particles residing within the cell volume ($\Delta V = (\Delta x)^3$, where Δx is the grid spacing) centered around each grid point ($m_p = \pi \rho_p d_p^3/6$ is the mass of a single particle and n_p is the number of particles within the cell volume).

The carrier phase is simulated by a Fourier pseudo-spectral method, and the particles are tracked individually in a Lagrangian manner. For a given mean shear (S) we have considered five cases to investigate the effects of one- and two-way coupling at various values for the particle time constant (τ_p) and the mass loading ratio (Φ_m = mass of the particles per unit volume/ρ_f), using as many as 6.67×10^5 particles on 96^3 collocation points. The velocity field was initialized as a random Gaussian, isotropic and solenoidal field in the Fourier space with a turbulence energy of 3 m^2/s^2 and a dissipation of 29.15 m^2/s^3. The particles were distributed randomly with velocities equal to that of the fluid at the position where they are placed. The fluid kinematic viscosity used was 721.8 kg/m^3, and the imposed strain rate on the fluid was 62.8 s^{-1}. The turbulence Reynolds number was 952. The resulting velocity gradient for the mean particle motion equals that of the carrier phase. To ensure the accuracy of the single phase flow simulation, successful comparisons have been established with the simulation results of Rogers et al. (1986), and the experimental data of Tavoularis and Corrsin (1981).

The modification of turbulence by the particles is illustrated in Fig. 1 by considering the temporal variations of the fluid turbulent kinetic energy ($k = \frac{1}{2}\langle u_i u_i \rangle$, where $\langle\ \rangle$ indicates the Eulerian ensemble average over the number of grid points) and its dissipation rate (ϵ). Both variables are normalized with their

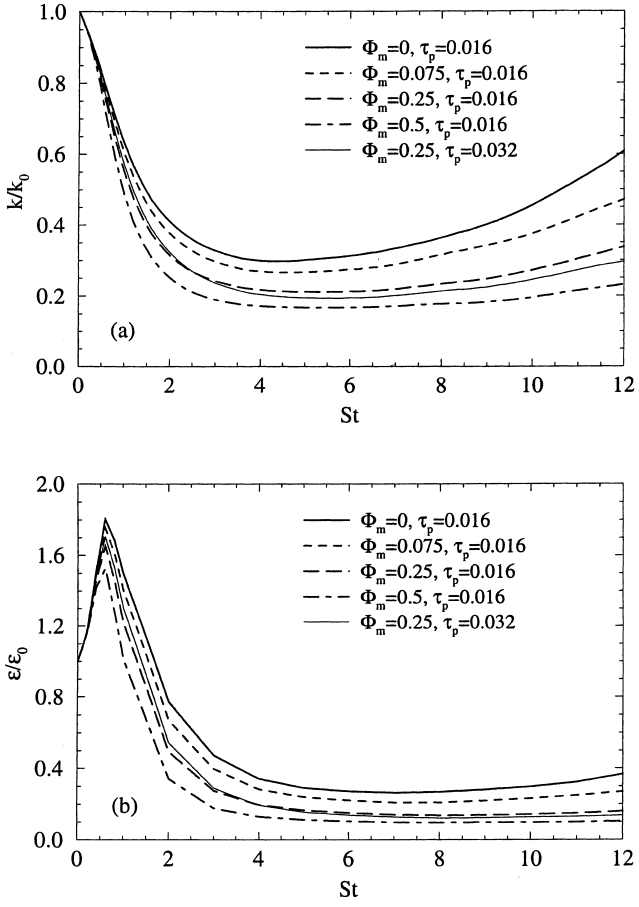

Fig. 1. Temporal variations of the fluid turbulent kinetic energy and its rate of dissipation. Both quantities are normalized with their initial values.

corresponding initial values denoted by subscript (0). For all of the cases, initially the fluid turbulent kinetic energy decays due to the absence of the off-diagonal (shear) Reynolds stress term. This term, along with the mean velocity gradient, are responsible for the production of energy in the streamwise direction. After the shear Reynolds stress component is produced by the action of the mean velocity gradient, the kinetic energy starts to increase ($\mathrm{St} > 4$). The primary effect of the particles on the fluid is to decrease the turbulent kinetic energy with respect to its single phase value. This is also the case for the dissipation rate as shown in Fig. 1(b). The decrease of the kinetic energy and its rate of dissipation in the presence of particles, suggests the existence of an extra dissipation which originates from the drag force.

The equation governing the particle turbulent kinetic energy ($k_p = \frac{1}{2}\langle\langle v_i v_i \rangle\rangle$, with $\langle\langle\ \rangle\rangle$ denoting the Lagrangian ensemble average) is

$$\frac{dk_p}{dt} = -\langle\langle v_1 v_2 \rangle\rangle S + \frac{\langle\langle f \rangle\rangle}{\tau_p}(\langle\langle u_i v_i \rangle\rangle - 2k_p). \tag{4}$$

In deriving Eq. (4), the triple correlations between f and velocity components have been neglected after analyzing the DNS data. The first term on the RHS of Eq. (4) represents a production by the mean velocity gradient while the second term is due to drag. The temporal evolution of these terms in Fig. 2 indicates that for all of the cases the term due to drag behaves as a dissipation and tends to balance the production. Obviously, during the initial times ($\mathrm{St} < 4$), the dissipation overcomes the production and the particle turbulent kinetic

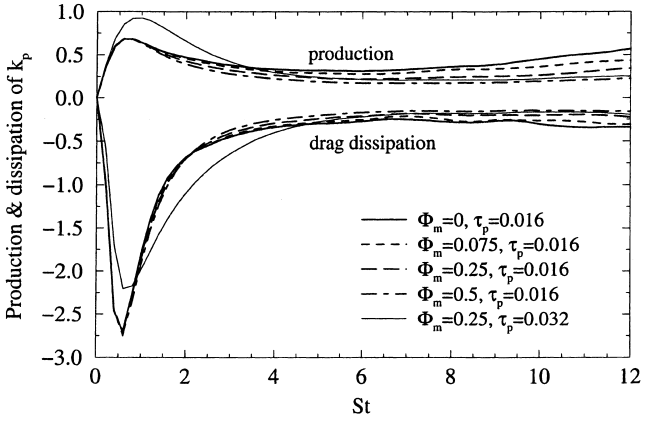

Fig. 2. Temporal variations of the production and drag dissipation terms appearing in the particle kinetic energy equation.

energy experiences a rapid decay, similar to those for the fluid. At longer times, Fig. 2 shows that the increase of the mass loading ratio results in the decrease of the magnitude of both the production and dissipation. However, the decrease of the production with the mass loading ratio occurs with a faster rate than that of the dissipation. As a result, the growth rate of the particle turbulent kinetic energy is decreased with the increase of the mass loading ratio. A comparison of cases with different particle time constant values (at the same mass loading ratio) reveals that the initial evolution of the production and the dissipation terms are more sensitive to the variations of the particle time constant, than are to the variations of the mass loading ratio. During the initial times, the increase of the particle time constant decreases the decay rate of the particle turbulence energy while at long times it results in the decrease of the growth rate of the kinetic energy.

The overall effects of the interaction between the carrier and dispersed phases are summarized in Table 1 which shows results at St = 12. It is seen that the turbulence non-dimensional time scale Sk/ϵ increases with mass loading indicating the turbulence becomes more sluggish. As observed from the components of the anisotropic tensors, $a^f_{ij} = \langle u_i u_j\rangle/k - 2\delta_{ij}/3$ and $a^p_{ij} = \langle\langle v_i v_j\rangle\rangle/k_p - 2\delta_{ij}/3$, the normal components of both the fluid and the particle velocity correlations become more anisotropic with increasing mass loading whereas the shear components decrease slightly. Also, the particle normal Reynolds stress in the flow direction is larger than that of the carrier fluid. This is in agreement with the theoretical results of Reeks (1993) and Liljegren (1993) and the LES results of Simonin et al. (1995), and is due to the lack of small scale dissipation in the dispersed phase as opposed to the fluid phase. Furthermore for large mass loading the kinetic energy of the particles becomes larger than that of the fluid.

Table 1
DNS results at St = 12

	$\tau_p = 0.016$			$\tau_p = 0.032$
Φ_m	0	0.25	0.5	0.25
Sk/ϵ	4.82	5.88	6.31	5.95
a^f_{11}	0.361	0.533	0.725	0.515
a^f_{22}	−0.291	−0.382	−0.453	−0.418
a^f_{12}	−0.324	−0.325	−0.309	−0.262
a^p_{11}	0.630	0.774	0.890	0.888
a^p_{22}	−0.417	−0.468	−0.509	−0.530
a^p_{12}	−0.414	−0.394	−0.359	−0.352
$\langle\langle v_1^2\rangle\rangle/\langle u_1^2\rangle$	1.037	1.181	1.147	1.197
$\langle\langle v_2^2\rangle\rangle/\langle u_2^2\rangle$	0.546	0.688	0.757	0.500
k_p/k	0.821	0.984	1.025	0.910

3. Reynolds stress closures

In this section a second-order moment Reynolds stress model is proposed for particle-laden flows that includes the effects of two-way coupling between the two phases. The predictions of the model are then compared with the DNS generated data. The model is based on the two-fluid treatment of two-phase flows. Similar to DNS, we consider the transport of an incompressible fluid (the carrier gas) laden with mono-size particles (the dispersed phase). The governing equations for both phases are expressed in the Eulerian frame by performing volume averaging. For a dilute dispersed phase, typically the volume fraction ($\hat{\Phi}$ = volume of particles per unit volume of fluid) $\sim\mathcal{O}(10^{-4})$; the transport equation for the carrier phase simplifies to Eq. (2) except the particle drag term becomes $\lambda\Phi(\hat{U}_i - \hat{V}_i)/\tau_p$, $\lambda = \rho_p/\rho_f$, due to the volume averaging process. We assume Stokes drag, and the effect of the carrier phase pressure on the particles is negligible. The volume averaged particle equation in the Eulerian form can be written as

$$\frac{\partial \hat{V}_i}{\partial t} + \hat{V}_j\frac{\partial \hat{V}_i}{\partial x_j} = \frac{1}{\tau_p}(\hat{U}_i - \hat{V}_i). \tag{5}$$

Following the standard Reynolds decomposition procedure, the flow variables are decomposed into the 'ensemble-mean' and fluctuations about the mean: $\hat{U}_i = U_i + u_i$, $\hat{V}_i = V_i + v_i$, $\hat{P} = P + p$ and $\hat{\Phi} = \Phi + \phi$; and mean flow equations can be obtained by averaging Eqs. (2) and (5). For the homogeneous shear flow considered here, the fluid velocity is specified with $V_i = U_i$ and with zero void fraction fluxes $\overline{u_i\phi}$ and $\overline{v_i\phi}$. The transport differential equations for other second-order moments are obtained from Eqs. (2) and (5) by standard methods:

$$\frac{\partial \overline{u_iu_j}}{\partial t} = -\overline{u_iu_l}\frac{\partial U_j}{\partial x_l} - \overline{u_ju_l}\frac{\partial U_i}{\partial x_l} + \psi_{ij} - \epsilon_{ij} - \frac{\Phi_m}{\tau_p} \times [\overline{u_i(u_j - v_j)} + \overline{u_j(u_i - v_i)}], \tag{6}$$

for the carrier phase Reynolds stress,

$$\frac{\partial \overline{v_iv_j}}{\partial t} = -\overline{v_iv_l}\frac{\partial V_j}{\partial x_l} - \overline{v_jv_l}\frac{\partial V_i}{\partial x_l} - \frac{1}{\tau_p}(2\overline{v_iv_j} - \overline{u_iv_j}, -\overline{u_jv_i}), \tag{7}$$

for the dispersed phase Reynolds stress, and

$$\frac{\partial \overline{u_iv_j}}{\partial t} = -\overline{u_iv_l}\frac{\partial V_j}{\partial x_l} - \overline{u_iv_j}\frac{\partial U_i}{\partial x_l} + \chi_{ij} + \frac{1}{\tau_p}(\overline{u_iu_j} - \overline{u_iv_j}) - \frac{\Phi_m}{\tau_p}(\overline{u_iv_j} - \overline{v_iv_j}), \tag{8}$$

for fluid-particle velocity covariance. In Eq. (6), $\psi_{ij} = \overline{(p/\rho_f)(\partial u_i/\partial x_j + \partial u_j/\partial x_i)}$ is the pressure–strain correlation, and $\epsilon_{ij} = \overline{2\nu(\partial u_i/\partial x_l)(\partial u_j/\partial x_l)}$ indicates the dissipation rate. In Eq. (8), $\chi_{ij} = \overline{(p/\rho_f)(\partial v_j/\partial x_i)}$ is the pressure-dispersed phase velocity gradient correlation. In these equations, the third-order correlations involving both the velocity and the void fraction fluctuations are neglected.

The pressure terms, ψ_{ij} and χ_{ij} are modeled similarly to the widely utilized closure of Launder, Reece and Rodi (LRR) (Launder et al., 1975). Utilizing Fourier transform methods the Poisson equation for the pressure can be solved resulting in expressions for ψ_{ij} and χ_{ij} in terms of integrals of two-point velocity correlations. The result for ψ_{ij} contains extra terms, involving fluid–particle velocity correlations, arising from the effects of the particles on the fluid. Following Launder et al. (1975) the pressure–strain term ψ_{ij} is formulated as a linear

polynomial of the velocity correlations. The coefficients of this polynomial are obtained by applying the constraints of symmetry, incompressibility, and normalization. The final result for homogeneous flows is

$$\Pi_{ij} = -C_{f1}\epsilon a^f_{ij} + \epsilon\left[\frac{4}{5}S^f_{ij} - 6C_{f2}\left(a^f_{ik}S^f_{kj} + a^f_{jk}S^f_{ki} - \frac{2}{3}a^f_{mn}S^f_{nm}\delta_{ij}\right) - \frac{4+14C_{f2}}{3}(a^f_{ik}\omega^f_{kj} + a^f_{jk}\omega^f_{ki})\right] + C_{f3}\frac{\lambda\Phi}{\tau_p}[2ka^f_{ij} - \overline{u_m v_m}(b^{fp}_{ij} + b^{fp}_{ji})], \quad (9)$$

where C_{f1}, C_{f2} and C_{f3} are empirical constants to be determined, $a^f_{ij} = \overline{u_i u_j}/k - 2\delta_{ij}/3$ and $b^{fp}_{ij} = \overline{u_i v_j}/\overline{u_m v_m} - \delta_{ij}/3$ are the normalized form of the fluid–fluid and the fluid–particle Reynolds stresses, respectively; and $S^f_{ij} = (k/2\epsilon)(\partial U_i/\partial x_j + \partial U_j/\partial x_i)$ and $\omega^f_{ij} = (k/2\epsilon)(\partial U_i/\partial x_j - \partial U_j/\partial x_i)$ are the strain rate and the rotation tensors of the carrier phase, respectively. In Eq. (9) the first two terms are the LLR closure for the slow and fast pressure–strain effects, respectively, and the last term depicts the particle effects. Following a similar procedure, a model is derived for the pressure-dispersed phase velocity gradient correlation

$$\chi_{ij} = -C_{fp1}\frac{\overline{u_i v_j}}{\tau} + C_{fp2}\overline{u_l v_j}\frac{\partial U_i}{\partial x_l} + C_{fp3}\frac{\lambda}{\tau_p}\Phi(\overline{u_i v_j} - \overline{v_i v_j}), \quad (10)$$

where $\tau = k/\epsilon$ is the carrier phase turbulent time scale, and C_{fp1}, C_{fp2}, and C_{fp3} are empirical constants.

Eqs. (9) and (10) indicate that the proposed closures involve six empirical constants which must be determined. The terms involving C_{f1} or C_{f2} in Eq. (9) are the equivalent of those in LRR. Thus, the magnitudes of these constants are set to be the same ($C_{f1} = 1.75$, $C_{f2} = -0.159$) to ensure that in the limit of one-way coupling Eq. (9) reduces to the equivalent LRR model for single phase flows. The magnitudes of the other four constants are determined by balancing the transport equations for all of the components of the fluid Reynolds stress tensor (Eq. (6)) and the fluid–particle covariance tensor (Eq. (8)). Note that all of the remaining terms in these equations as well as the terms in models of pressure–strain correlation and pressure–particle velocity gradient correlation are computable directly from the Lagrangian simulations. By considering all of the components and all of the cases a large data bank is furnished to determine and to optimize the values of the remaining four constants. A sample case is shown in Fig. 3 for the energy budget of $\langle\langle u_1 v_1\rangle\rangle$ for $\Phi_m = 0.25$ and $\tau_p = 0.032$ s. In this figure, the production, the dissipation rate, and the contribution from drag are calculated from DNS. The values of the pressure-dispersed phase velocity gradient are calculated from the proposed models. The term LHS indicates the derivative of the energy component and is obtained from DNS. This value is compared with $\sum$RHS which is the sum of the production, dissipation rate, and drag contribution (from DNS), and the pressure term (from models). It is observed that the general agreement between the LHS and the $\sum$RHS is good, especially for St > 2 when the turbulence is well-developed. Similar comparisons have also been performed for other components for all of the cases. The final (optimized) values of the empirical constants are given in Table 2.

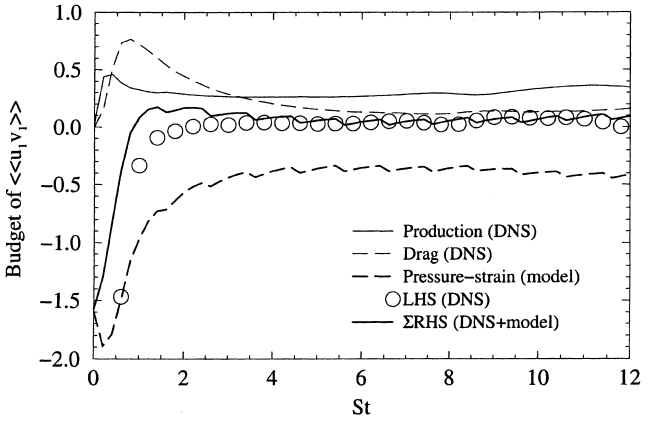

Fig. 3. Budget of $\langle\langle u_1 v_1\rangle\rangle$ from the case with $\Phi_m = 0.25$ and $\tau_p = 0.032$ s.

The final form of the transport equations for all of the components of the Reynolds stress tensors constitute a set of Reynolds stress models for particle-laden homogeneous shear flows. To close, an equation must be provided for the dissipation rate of the fluid turbulent kinetic energy. The modeled dissipation rate equation can be rationalized from the exact equation for the dissipation rate as obtained from Eq. (2). For the present case this equation includes an additional term, $(2\lambda\Phi/\tau_p)\left[\nu\overline{(\partial u_i/\partial x_j)(\partial u_i/\partial x_j)} - \nu\overline{(\partial u_i/\partial x_j)(\partial v_i/\partial x_j)}\right]$, due to coupling with the dispersed phase. In this expression the first term is the dissipation ϵ and the second term is modeled as the relaxation of the trace of fluid–particle velocity correlation tensor, i.e, $C_{\epsilon 3}\overline{u_m v_m}/\tau$. The final form of the modeled transport equation for the dissipation rate for homogeneous flow is expressed as

$$\frac{\partial\epsilon}{\partial t} = -C_{\epsilon 1}\frac{\epsilon}{k}\overline{u_1 u_2}\frac{\partial U_1}{\partial x_2} - C_{\epsilon 2}\frac{\epsilon^2}{k} - \frac{\epsilon}{k}\frac{\lambda\Phi}{\tau_p}(2k - C_{\epsilon 3}\overline{u_m v_m}), \quad (11)$$

where $C_{\epsilon 1}$, $C_{\epsilon 2}$, and $C_{\epsilon 3}$ are constants. The values for $C_{\epsilon 1}$ and $C_{\epsilon 2}$ are taken from their single-phase equivalents; $C_{\epsilon 1} = 1.45$ and $C_{\epsilon 2} = 1.85$. The value of constant $C_{\epsilon 3} = 0.8$ is found by comparison with DNS data.

The data generated by DNS for the fluid, particle, and fluid–particle Reynolds stresses are used to assess the Reynolds stress model. In this assessment the stress and the dissipation rate values at $St = 2$ are taken from DNS as initial values. This time is chosen as the initial time in order to allow the flow and the particles to reach a dynamic equilibrium. All of the cases have been considered; however, the results of only two cases are presented here. Similar trends were obtained for cases with different mass-loading ratios and particle relaxation times.

The numerical procedure involves simultaneous integration of 14 coupled equations (13 for Reynolds stresses and 1 for the dissipation rate). The time derivative term is discretized by a backward finite difference scheme. The decay term is evaluated by averaging between the two successive time levels in order to expedite convergence. By performing two iterations at each time level the resulting technique is similar to the Crank–Nicholson method.

Table 2
Empirical constants

Constant	Magnitude	Basis for choice
C_{f1}	1.75	Launder et al. (1975)
C_{f2}	−0.159	Launder et al. (1975)
C_{f3}	0.5	Budget of $\overline{u_i u_j}$
C_{fp1}	2.5	Budget of $\overline{u_i v_j}$
C_{fp2}	0.5	Budget of $\overline{u_i v_j}$
C_{fp3}	0.2	Budget of $\overline{u_i v_j}$
C_{ϵ_1}	1.45	Standard k–ϵ
C_{ϵ_2}	1.85	Standard k–ϵ
C_{ϵ_3}	0.8	Overall performance of RSM

First we consider the case with one-way coupling ($\Phi_m = 0$) for $\tau_p = 0.016$ s. The model predictions (lines) are compared with DNS results (symbols) in Fig. 4 for all of the components. The overall agreement is very good; the particle Reynolds stress components (Fig. 4(b)) show the best overall agreements. This is expected as the transport equations for the particle Reynolds stresses involve no modeling. Small deviations observed in Fig. 4(b) is due to $\overline{u_i v_j}$ terms. It is noted that the shear components which are of primary importance are predicted very closely to DNS. For this one-way coupling case, Fig. 4(a) essentially evaluates the performance of the LRR model. Some deviations are observed in the streamwise ($\overline{u_1 u_1}$) component but other components are in reasonably good agreements.

The effects of two-way coupling at $\Phi_m = 0.25$ and $\tau_p = 0.016$ s are portrayed in Fig. 5. Again the agreement between the model predictions and DNS results is very promising.

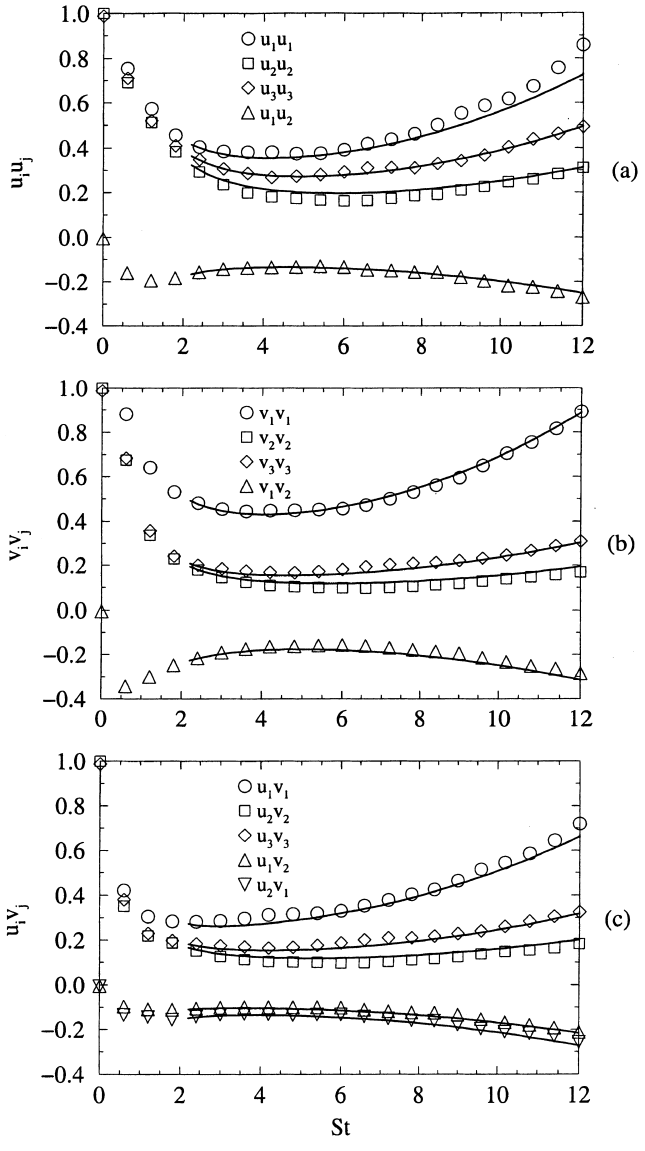

Fig. 4. Comparisons of the Reynolds stress model predictions (lines) with DNS data (symbols) for components of the fluid, particle and fluid–particle Reynolds stress tensors in the case with one-way coupling at $\tau_p = 0.016$ s.

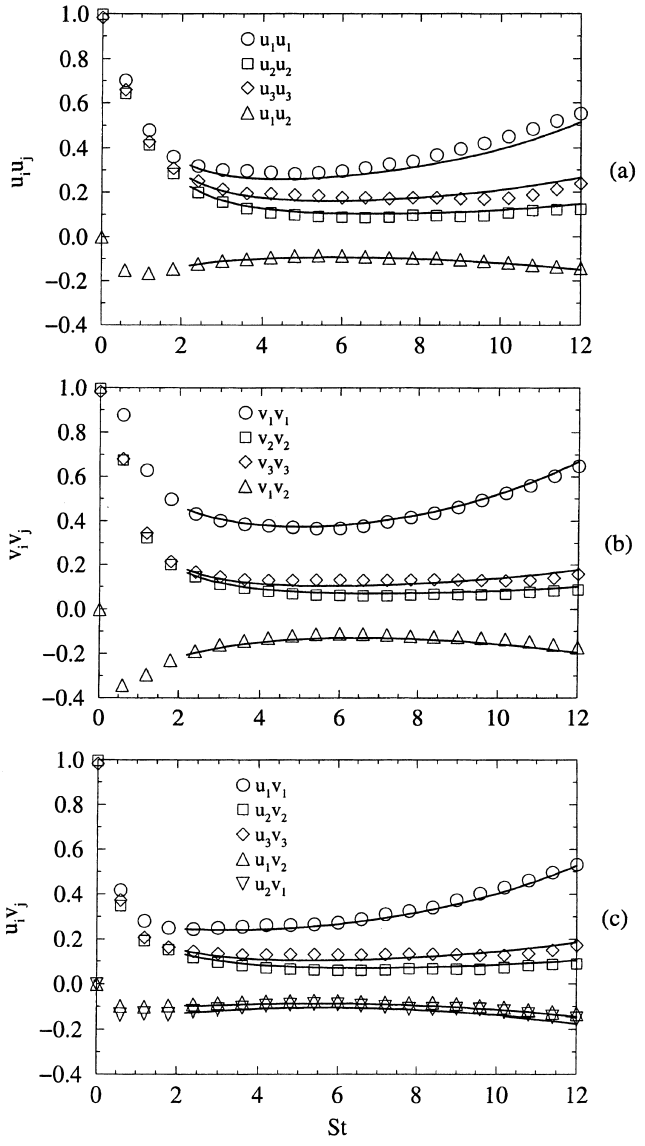

Fig. 5. Comparisons of the Reynolds stress model predictions (lines) with DNS data (symbols) for components of the fluid, particle and fluid–particle Reynolds stress tensors for $\Phi_m = 0.25$ and $\tau_p = 0.016$ s.

Similar to the case with one-way coupling, the largest deviations are observed in the streamwise direction, especially for the fluid. Finally, Fig. 6 shows that the dissipation rate is also calculated very closely to DNS results, for the two cases.

4. Concluding remarks

This work deals with direct numerical simulation of particle-laden homogeneous shear flow, and proposes a new Reynolds stress model for statistical prediction of two-phase flows. The DNS results are used to assess the performance of the RSM. Reasonable agreement between model and DNS results are observed, especially for the shear (off-diagonal) components which are of primary importance. A very important feature of model is that the effects of the two-way coupling are included in every aspect of the formulation. Work is underway in implementation of the proposed RSM in homogeneous plane-strain flows and their validations via DNS.

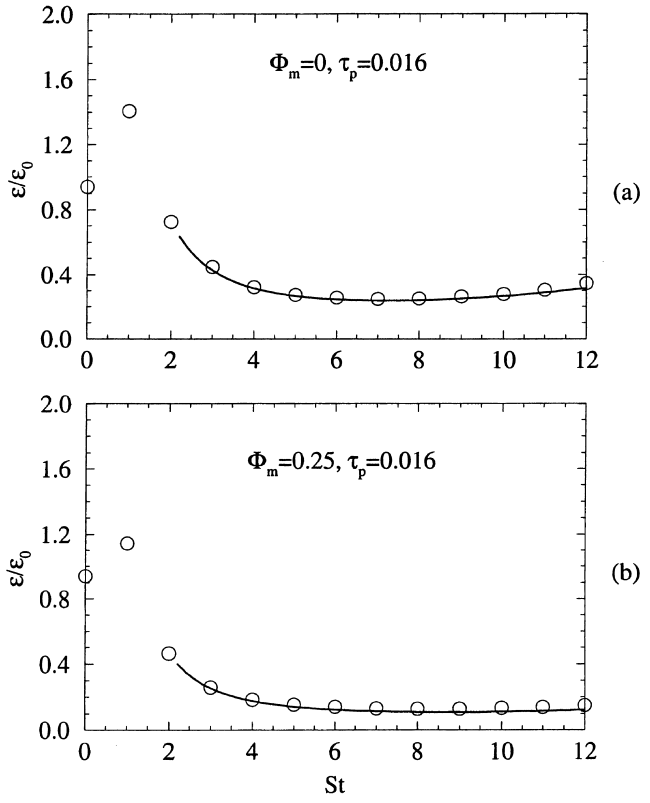

Fig. 6. Comparisons of the Reynolds stress model predictions (lines) with DNS data (symbols) for the dissipation rate of the fluid turbulent kinetic energy. (a) $\Phi_m = 0$, $\tau_p = 0.016$ s, (b) $\Phi_m = 0.25$, $\tau_p = 0.016$ s.

References

Chen, C.P., Wood, P.E., 1986. Turbulence closure modeling of the dilute gas–particle axisymmetric jet. AIChE J. 32, 163–166.

Crowe, C.T., Troutt, T.R., Chung, J.N., 1996. Numerical models for two-phase turbulent flows. Ann. Rev. Fluid Mech. 28, 11–43.

Elghobashi, S.E., Abou-Arab, T.W., 1983. A two-equation turbulence model for two-phase flows. Phys. Fluids 26, 931–938.

Elghobashi, S., Truesdell, G.C., 1992. Direct simulation of particle dispersion in a decaying isotropic turbulence. J. Fluid Mech. 242, 655–700.

Elghobashi, S., Truesdell, G.C., 1993. On the two-way interaction between homogeneous turbulence and dispersed solid particles. I: Turbulence modification. Phys. Fluids 5, 1790–1801.

Launder, B.E., Reece, G.J., Rodi, W., 1975. Progress in the development of a Reynolds-stress turbulence closure. J. Fluid Mech. 68, 537–566.

Liljegren, L.M., 1993. The effect of a mean fluid velocity gradient on the streamwise velocity variance of a particle suspended in a turbulent flow. Int. J. Multiphase Flow 19, 471–484.

McLaughlin, J.B., 1989. Aerosol particle deposition in numerically simulated channel flow. Phys. Fluids 1, 1211–1224.

Reeks, W.M., 1993. On the constitutive relations for dispersed particles in nonuniform flows. I: Dispersion in a simple shear flow. Phys. Fluids 5, 750–761.

Riley, J.J., Patterson, G.S., 1974. Diffusion experiments with numerically integrated isotropic turbulence. Phys. Fluids 17, 292–297.

Rogers, M.M., Moin, P., Reynolds, W.C., 1986. The structure and modeling of the hydrodynamic and passive scalar fields in homogeneous turbulent shear flow. Department of Mechanical Engineering TF-25, Stanford University, Stanford, CA.

Shih, T.-H., Lumley, J.L., 1986. Second-order modelling of particle dispersion in a turbulent flow. J. Fluid Mech. 163, 349–363.

Simonin, O., Deutsch, E., Boivin, M., 1995. Large eddy simulation and second-moment closure model of particle fluctuating motion in two-phase turbulent shear flows. In: Durst, F., Kasagi, N., Launder, B.E., Schmidt, F.W., Whitelaw, J.H. (Eds.), Turbulent Shear Flows 9, Springer, Berlin, pp. 85–115.

Squires, K.D., Eaton, J.K., 1991a. Measurements of particle dispersion obtained from direct numerical simulations of isotropic turbulence. J. Fluid Mech. 226, 1–35.

Squires, K.D., Eaton, J.K., 1991b. Preferential concentration of particles by turbulence. Phys. Fluids 3, 1169–1178.

Tavoularis, S., Corrsin, S., 1981. Experiments in nearly homogenous turbulent shear flow with a uniform mean temperature gradient. Part 1. J. Fluid Mech. 104, 311–347.

Yeh, F., Lei, U., 1991. On the motion of small particles in a homogeneous turbulent shear flow. Phys. Fluids 3, 2758–2776.

Zhou, L.X., Liao, C.M., Chen, T., 1994. A unified second-order-moment two-phase turbulent model for simulating gas–particle flows. In: Crowe, C.T., Johnson, R., Prosperetti, A., Sommerfeld, M., Tsuji, Y. (Eds.), Numerical Methods in Multiphase Flows, ASME, FED-Vol. 185, NY, pp. 307–313.